STUDY OF THE STRUCTURAL AND ELECTRONIC PROPERTIES OF Fe DOPING STANENE NANORIBBONS: A CASE DFT

Nguyen Thanh Tung[1,2,*], *Tran Cong Phong*[2,3]

[1]Institute for Advanced Study in Technology, Ton Duc Thang University, Ho Chi Minh City,Vietnam .
[2]Atomic Molecular and Optical physics Research Group, Institute for Advanced Study in Technology, Ton Duc Thang University, Ho Chi Minh City, Vietnam .
[3]Faculty of Electrical and Electronics Engineering, Ton Duc Thang University, Ho Chi Minh City, Vietnam.

*Corresponding Author: Nguyen Thanh Tung (Email: nguyenthanhtung.st@tdtu.edu.vn)
(Received: 20-February-2025; accepted: 27-May-2025; published: 30-June-2025)
http://dx.doi.org/10.55579/jaec.202592.488

Abstract. *The structural and electronic properties of armchair stanene nanoribbons (ASnNRs) doped with iron (Fe) atoms were systematically investigated using density functional theory (DFT) calculations. A comprehensive first-principles analysis was performed, including calculations of formation energy, optimized structural parameters, electronic density of states (DOS, PDOS), band structure, and spatial charge density distribution. Various Fe doping configurations were considered, including single-atom substitutions at the top-1Fe and valley-1Fe positions, as well as two-atom doping in the ortho, meta, and para configurations, and a 100% substitution model where Fe and Sn atoms alternate. The pristine ASnNR was found to be non-magnetic with a band gap of 0.26 eV . Upon Fe doping, most configurations exhibited semiconducting behavior with narrow band gaps for instance, 0.24 eV in the valley-1Fe configuration, and down to 0.24 eV and 0.14 eV in the ortho case indicating potential for application in infrared radiation sensors. In other configurations, the band gap was reduced nearly to zero. Additionally, all doped systems exhibited significant magnetic moments, with the highest value of 11.3 μB observed in the 100% Fe-doped structure. These results suggest promising potential for Fe-doped ASnNRs in future spintronic and nanoelectronic device applications.*

Keywords: *Stanene nanoribbons; Fe doping stanene; Electronic properties; Magnetic properties; Spintronics.*

1. Introduction

Nanoribbons are a class of one-dimensional (1D) nanomaterials characterized by a narrow width in the nanometer scale and a length extending up to several micrometers [1]. Structurally, nanoribbons exhibit properties that lie at the intersection between two-dimensional (2D) and 1D materials [2], resulting in a range of unique and enhanced characteristics. These include exceptional electrical conductivity, high mechanical strength, and pronounced quantum confinement effects [3]. Commonly studied nanoribbons include graphene nanoribbons (GNRs), silicene nanoribbons, and more recently, stanene nanoribbons. These materials have attracted considerable interest for applications in electron-

ics, optics, sensors, and energy storage technologies. Notably, nanoribbons not only retain many of the superior properties of their corresponding 2D forms but also offer tunability through variations in shape, size, and fabrication methods [4].

Stanene, a monolayer of tin atoms arranged in a honeycomb lattice analogous to graphene and silicene, represents an emerging 2D material with distinctive electronic and insulating properties [5]. Among its most remarkable characteristics is its potential as a topological insulator at room temperature, featuring robust edge states immune to non-magnetic impurities [6]. Additionally, stanene exhibits Dirac-like electronic behavior, enabling high carrier mobility and tunable bandgaps, along with excellent thermoelectric properties attributed to its large thermoelectric coefficient qualities that suggest promising applications in thermoelectric energy conversion devices [7].

To enhance or modify stanene's intrinsic properties, techniques such as adsorption and doping have been extensively employed. Adsorption, involving the attachment of atoms, molecules, or ions onto the surface of stanene, can profoundly alter its electronic, magnetic, and optical properties. For example, gas adsorption studies have demonstrated that stanene can adsorb gases such as O_2, H_2, NH_3, and CO_2, resulting in modifications to the electronic structure and potential applications in gas sensing technologies [8]. Moreover, metal atom adsorption (e.g., Li, Na, or K) has revealed stanene's suitability as an electrode material for metal-ion batteries, owing to its high capacity for energy storage [9].

Doping, the intentional incorporation of foreign atoms into the stanene lattice, is another effective strategy to tailor its properties. Doping with group V elements such as Bi or Sb has been shown to enhance topological insulating behavior while improving structural stability [10]. Similarly, the introduction of transition metal dopants, including Mn and Co, can induce ferromagnetism, opening pathways for spintronic device applications [11]. Non-metallic dopants such as F and Cl offer an additional route to modulate the bandgap, enabling material property tuning for specific application requirements. Several recent studies have significantly expanded the understanding of adsorption and doping in stanene. For instance, Li et al. (2021) reported enhanced NH_3 sensing capabilities in stanene attributed to charge density redistribution upon gas adsorption [12]. Additionally, the incorporation of Na, Mg, and Al atoms was found to stabilize magnetic states with potential in magnetic data storage applications [13] and CO, F_2, NO_2 adsorbed SnNRs [14], while co-doping with metallic elements improved stanene's thermoelectric performance, further promoting its use in energy conversion technologies [15].

Although numerous previous studies have focused on the adsorption of various species on the stanene surface, carried out by different research groups as well as our team in publications from 2025 [13, 14], particular attention has been given to the doping of Fe into Stanene/Cu (111). This work combined density functional theory (DFT) calculations with experimental investigations based on the Numerical Renormalization Group (NRG) method. The detailed results demonstrated that Fe doping at the monomer, dimer, and trimer atomic levels significantly modifies the topological properties and induces magnetic phase transitions [16, 17]. In the present study, we aim to further examine and clarify the changes in the electronic and magnetic properties of stanene nanoribbons upon Fe doping at various substitutional positions. We investigate the associated electronic behavior, adsorption energies, and further assess the magnetic density and induced magnetic moments in each specific configuration.

By systematically analyzing the modulation of the bandgap and the magnetic behavior induced by Fe incorporation, this study seeks to evaluate the potential of Fe-doped ASnNRs for future applications in semiconductor devices, particularly spin-based electronic devices.

2. Calculation method

Density functional theory (DFT) calculations were performed using the Vienna Ab initio Simulation Package (VASP) [18]. The com-

putational models were constructed to account for both the concentration and spatial distribution of adatoms. The exchange–correlation interactions were described using the Perdew–Burke–Ernzerhof (PBE) functional [19] within the framework of the generalized gradient approximation (GGA) [20]. Electron–ion interactions were treated with the projector augmented-wave (PAW) method [21]. A plane-wave basis set with an energy cutoff of 400 eV was employed. Structural relaxations were conducted using a Monkhorst–Pack [22] k-point mesh of 12×1×1, while electronic structure calculations utilized a denser grid of 100×1×1. The convergence criterion for the Hellmann–Feynman forces [23] acting on each atom was set to 0.01 $eV/\overset{0}{A}$.

We calculate the adsorption energy after fusion using the following formula in Eq. 1:

$$E_{Form} = E_{tot} + E_{pristine} + nE_{Sn} - nE_{Fe} \quad (1)$$

where the E_{tot}, $E_{pristine}$, E_{Sn}, and E_{Fe} are the ground state energy of the Fe substituted ASnNR structures, pristine ASiNR, Sn atoms replaced by Fe adatoms in the pristine system, and isolated Fe adatoms, respectively and n is the number of the Fe substitution atoms.

3. Results and discussion

3.1. Structure properties

In this study, a computational model of an armchair stanene nanoribbon (ASnNR) with a Miller index of N = 6 was constructed, consisting of 12 Sn atoms and 4 H atoms in the initial pristine structure, forming a hexagonal honeycomb lattice. Hydrogen atoms were introduced at the ribbon edges to stabilize the structure, tune the electronic properties, suppress edge-induced magnetic effects, and reduce the chemical reactivity of the boundaries. The doping model was designed by substituting Fe atoms at various Sn positions, including ortho, para, meta, top-1Fe, valley-1Fe, and 100% Fe replacement configurations, as referenced in previous studies [24–26] (see Fig. 1). The initial Sn–Sn bond length prior to structural optimization was set to 2.82 $\overset{0}{A}$, consistent with values reported for nanoscale stanene.

The structural modifications of the ASnNR substrate following Fe doping in different configurations were analyzed, as presented in Fig. 2 and Table 1. A comparison between Fig. 1 and Fig. 2 reveals that most doping configurations induce noticeable structural distortions, particularly in the side view. Among them, the ortho and para configurations exhibited the largest out-of-plane deformations of 0.32 $\overset{0}{A}$ and 0.45 $\overset{0}{A}$, respectively, compared to a flat pristine nanoribbon.

Due to the strong interaction between neighboring Sn and Fe atoms, the Sn–Sn bond lengths were significantly altered after doping, with the para configuration reducing from the initial 2.82 $\overset{0}{A}$ to 2.73 $\overset{0}{A}$. In contrast, the Sn–Fe bond lengths exhibited relatively minor fluctuations across different doping cases, stabilizing at an average value of approximately 2.55 $\overset{0}{A}$. Local lattice distortions were further enhanced by elongation of adjacent Sn–Fe bonds in configurations containing closely positioned Fe atoms, particularly in the ortho case, where adjacent Fe–Fe bonds contracted to 2.11 $\overset{0}{A}$.

Furthermore, the bond angles between adjacent Sn atoms (Sn–Sn–Sn) were also affected by Fe incorporation, increasing from the pristine value of 108.05° to 123.50° and 121.57° in the ortho and para configurations, respectively. These results indicate that substituting Sn atoms with Fe atoms leads to moderate lattice distortions and bond rearrangements while maintaining the overall integrity of the hexagonal crystal structure, supported by the high formation energies associated with these doped systems.

3.2. Electrical properties

The energy band structure (BAND) and projected density of states (PDOS) of the pristine ASnNRs substrate provide crucial insights into its electronic configuration. Tin (Sn) exhibits an electronic configuration of [Kr] $4d^{10}5s^25p^2$, with Sn atoms interconnected through inherently unstable σ bonds that are susceptible to breaking under external chemical influences. As shown

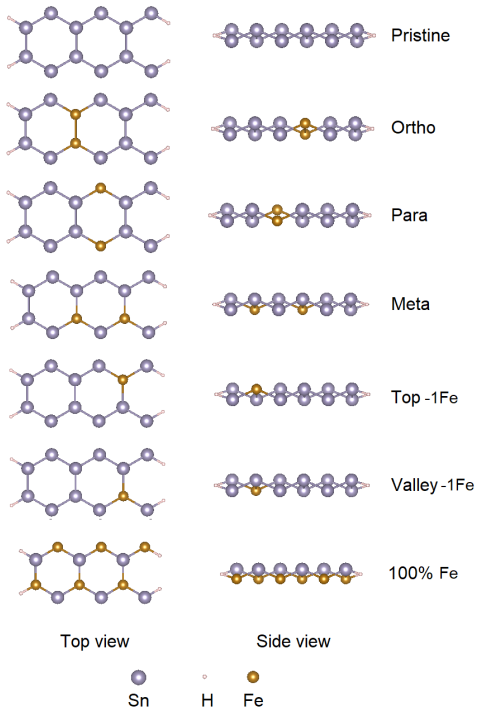

Fig. 1: Initial structure of Fe doped cases with ASnNRs.

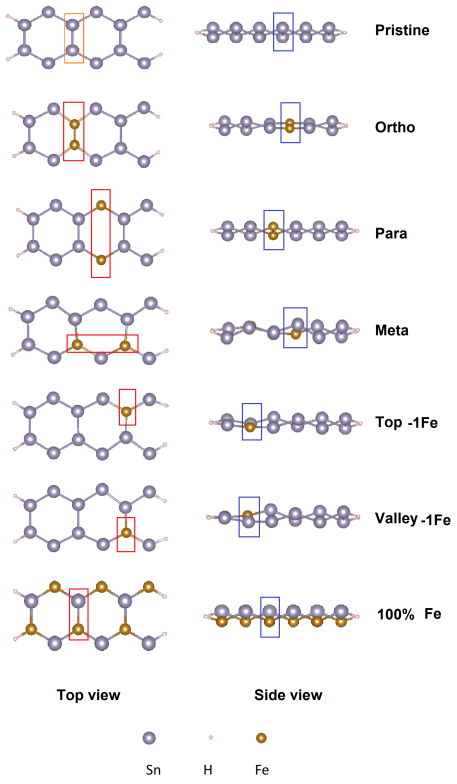

Fig. 2: The models of the structure after doping Fe atoms for Sn at seven different cases.

in Fig. 3, the PDOS analysis reveals that the contribution from Sn(4d) orbitals is negligible, while the electronic states are predominantly derived from the Sn(5s) and Sn(5p) orbitals. For clarity, the states are categorized into Sn(s), Sn(p), and Sn(d) components. The DOS components of the ASnNRs substrate (see Fig. 3), plotted from the total energy states corresponding to spin-up and spin-down configurations, exhibit an almost symmetric distribution around the Fermi level. This balance between the spin-up and spin-down states indicates that the pristine ASnNRs system is non-magnetic, as no significant spin polarization is observed in the electronic states. Furthermore, the nearly overlapping spin-resolved DOS curves confirm that the total magnetic moment is approximately zero, reaffirming the absence of intrinsic magnetism in the undoped ASnNRs material. This indicates the absence of spin splitting and confirms that the system possesses no net magnetic moment, demonstrating its intrinsic non-magnetic behavior. Such a result suggests that, without the presence of magnetic ASnNRs remain spin-degenerate, leading to a non-magnetic ground state.

The computed $PDOS$ results indicate that the Sn(s) states, represented by the wine-colored line, exhibit a broad distribution across the energy range from $+4$ eV to -8 eV, with notable peaks at approximately -4.40 eV, -5.20 eV, and -5.50 eV, corresponding to the deep valence band region. In contrast, the Sn(p) states, depicted by the green line, are primarily localized around the Fermi level, reaching a significant peak near -1.40 eV. Meanwhile, the Sn(d) states, indicated by the red line, contribute minimally to the overall electronic structure due to their lower energy and limited density near the Fermi level. The calculated electronic band gap for the pristine $ASnNRs$ structure with N = 6 was determined to be 0.26 eV (see Table 1), confirming its narrow-gap semiconducting nature.

To explore the electronic behavior of Fe-doped ASnNRs, we investigated the substitution of Sn atoms with Fe atoms, where Fe possesses an electronic configuration of [Ar] $3d^6 4s^2$. The valence $3d$ and $4s$ orbitals of Fe play a critical role in charge transfer processes and significantly influence the system's electronic structure. By examining the corresponding energy band structures and projected $PDOS$, the contributions from Fe(s), Fe(p), and Fe(d) orbitals can be clearly distinguished across different doping configurations, providing a detailed understanding of how Fe incorporation modulates the electronic properties of ASnNRs.

For the ortho configuration (see Fig. 4.a and Fig. 5.a), the results indicate that, apart from a few intense peaks near the lower valence band, the energy distribution of Sn(s), Sn(p), and Sn(d) orbitals remains largely unchanged compared to the pristine structure (see Fig. 3a, Fig. 3.b and Fig. 3.c). Notably, the Fe(d) orbital exhibits strong contributions at -2.05 eV, -2.25 eV, and -2.85 eV, while Fe(s) and Fe(p) orbitals contribute negligibly due to their low energy states. This redistribution of electronic states significantly affects the band gap, reducing its width to 0.14 eV, highlighting the influence of Fe doping on the material's electronic properties.

In the para configuration (see Fig. 4.b), the electronic states of Sn(s), Sn(p), and Sn(d) orbitals remain largely unchanged compared to the pristine structure. However, significant modifications are observed in the Fe(d) states, with the most pronounced peaks shifting to -0.75 eV and -0.3 eV. Additionally, the peak intensity of Fe(d) orbitals decreases sharply from 13 to 8 states/eV per unit cell. These Fe(d) states dominate the electronic structure near the Fermi level, effectively overshadowing contributions from Sn-based orbitals. The substantial involvement of Fe(d) orbitals in the electronic states near the Fermi level leads to a complete closure of the band gap, indicating a transition to metallic behavior. The band gap of a material plays a crucial role in determining its electronic properties, particularly its semiconducting or metallic behavior. In the case of Fe-doped ASnNRs, the substitution of Sn with Fe at different positions alters the orbital interactions between Fe and Sn atoms, leading to distinct changes in the electronic structure. When Fe replaces Sn at the or-tho position, the Fe atoms interact more strongly with their neighboring Sn atoms through d–p hybridization. This interaction significantly modifies the electronic structure, particularly near the Fermi level. The Fe(d) orbitals contribute to the formation of electronic states, but they do not completely fill the band gap. As a result, the material retains a narrow band gap of 0.14 eV, indicating that the system remains a semiconductor with some metallic characteristics. The partial closure of the band gap reflects the strong interaction between the Fe(d) orbitals and the Sn(p) orbitals, which alters the electronic configuration without fully turning the system into a metal. In contrast, when Fe substitutes Sn at the meta or para positions, the interaction between the Fe and Sn atoms is weaker. The Fe(d) orbitals still influence the electronic structure, but their contribution is less pronounced compared to the or-tho position. This weaker interaction leads to the complete closure of the band gap, resulting in a metallic behavior with a band gap of 0 eV. The electronic states created by Fe(d) orbitals are more localized and lead to an overlap of electronic states at the Fermi level, effectively closing the gap. Therefore, both meta and para configurations exhibit metallic behavior due to the stronger influence of Fe(d) states near the Fermi level. The magnetic properties of a material are closely related to the distribution and interaction of electron spins. In the case of Fe-doped ASnNRs, the magnetic moment depends on the extent to which Fe atoms influence the spin alignment within the material. Despite the presence of a narrow band gap of 0.14 eV at the or-tho position, the magnetic moment decreases. This is due to the strong d-p hybridization between the Fe(d) and Sn(p) orbitals. When Fe atoms interact strongly with the Sn atoms, electron redistribution occurs, leading to a less pronounced magnetic moment. The electron sharing between Fe and Sn reduces the magnetic polarization of Fe, resulting in a weaker magnetic moment. As a result, the or-tho configuration exhibits a decrease in the overall magnetic moment, even though the material remains semiconducting. At the meta and para positions, the weaker interaction between Fe and Sn means

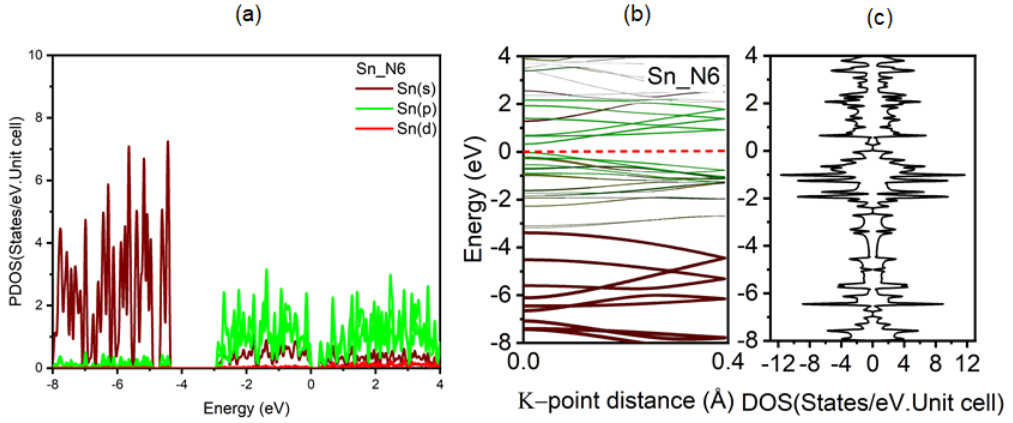

Fig. 3: The structure (a) PDOS, (b) BAND, and (c) DOS of pristine ASnNRs.

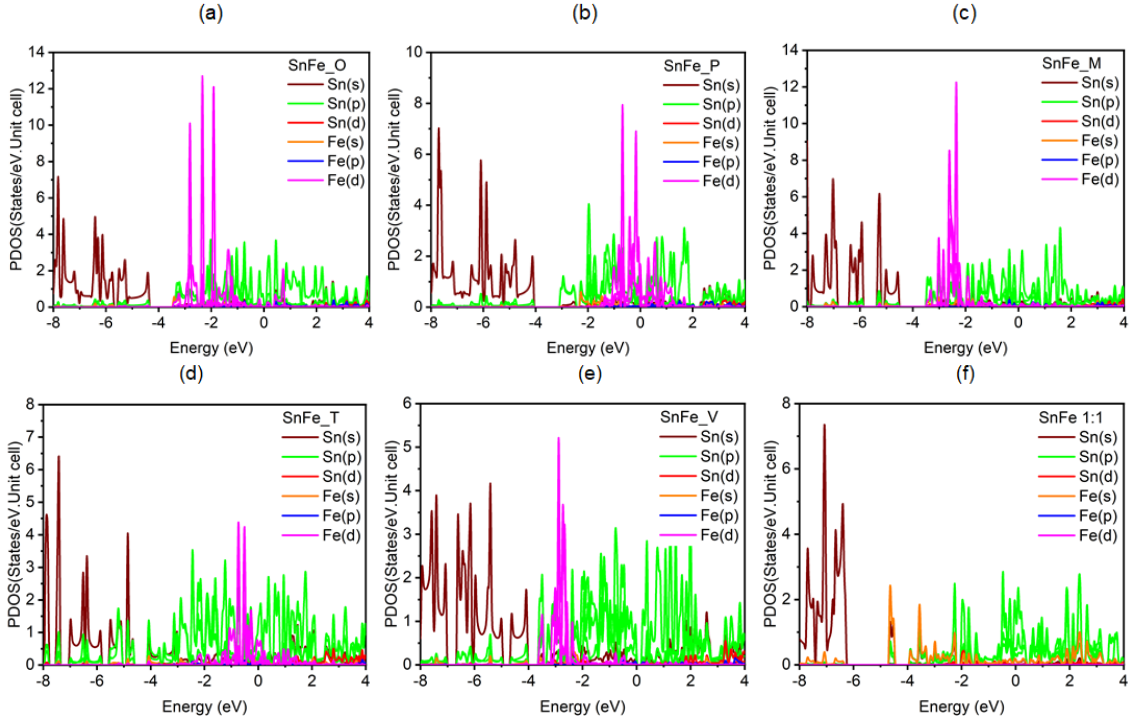

Fig. 4: The PDOS of six cases Fe doped ASnNRs.

that the magnetic moment is less affected by hybridization. The Fe atoms retain their magnetic properties more effectively, and as a result, the magnetic moment remains higher compared to the or-tho configuration. Since the band gap is fully closed in these configurations, the system behaves more like a metal with less influence on the spin distribution, leading to a more stable magnetic moment.

Based on the DOS states of the six Fe substitution configurations in ASnNRs (as shown in Fig. 5), it can be observed that the total electronic states exhibit the strongest intensity in the spin-down channel for the SnFe_T (see Fig. 5.d) case. In general, the overall DOS intensities in all Fe-doped systems are lower than those of the pristine ASnNRs substrate (see Fig. 3). However, a more significant observation is that

all Fe-doped configurations clearly exhibit spin polarization, as evidenced by the imbalance between the spin-up and spin-down states, indicating that the systems possess magnetic characteristics. This effect is most pronounced in the 100% Fe-doped configuration, where the spin-up and spin-down energy levels are distinctly different throughout the entire energy range.

The other doping configurations, including Ortho, Meta, Para, Top-1Fe, and Valley-1Fe, also display asymmetric distributions of spin-resolved energy states, with each case exhibiting unique features. As summarized in Table 1, the calculated total magnetic moments for these systems range from 4.0 to 5.99 μB, while the 100% Fe-doped system reaches a significantly higher value of 11.3 μB. This confirms that substituting Fe atoms into the ASnNRs lattice induces notable magnetic properties, and the degree of spin polarization as reflected by the difference in spin-up and spin-down DOS curves is closely correlated with the concentration and distribution of Fe dopants.

The projected density of states and BAND analyses for the meta configuration (denoted as SnFe_M, see Fig. 4.c and Fig. 5.c) reveal that the Sn(s) and Sn(p) orbitals exhibit minimal changes in both energy distribution and peak positions compared to the pristine ASnNRs structure. The most notable modifications appear at the lower region of the valence band. In particular, Fe(d) orbitals emerge prominently between -2 eV and -3 eV, a feature consistent with the ortho doping case. The relatively high adsorption energy of -8.25 eV indicates that this configuration is highly stable, maintaining a substantial magnetic moment of 5.99 μB, while bond lengths and bond angles remain largely unaltered relative to the pristine structure. For the valley configuration SnFe_V (see Fig. 5.e), where a single Sn atom at the valley position of the ASnNR is replaced by an Fe atom, the PDOS data indicates that the Sn(5s) orbitals remain widely distributed between -8 eV and 4 eV, though their peak intensities are lower compared to both the pristine structure and the top-doped counterpart.

The Sn(5p) states are nearly unchanged in both the valley and top configurations, implying that the primary influence of Fe doping stems from the introduction of Fe(d) states and their interaction with Sn orbitals. Notably, in the Valley-1Fe configuration, the Fe(d) orbitals generate a sharp localized peak at approximately -2.90 eV, a position considerably distant from the Fermi level. This positioning of the Fe(d) peak signifies a limited direct contribution to states at or near the Fermi level, which consequently preserves a narrow band gap of 0.24 eV. The restricted influence of Fe(d) states in valley-1Fe on the charge density near the conduction band minimum and valence band maximum accounts for the retention of semiconducting behavior, despite the presence of magnetic dopants. Furthermore, the calculated adsorption energy for this configuration is moderate at -8.25 eV, indicating stable Fe incorporation without inducing excessive structural distortions.

The associated magnetic moment remains high at 5.99 μB, reinforcing the potential magnetic functionalities of this system while maintaining a semiconducting band gap. In contrast, the top configuration SnFe_T case (see Fig. 5.d), where an Fe atom substitutes a Sn atom at the top lattice site, displays markedly different behavior. The Sn(5s) orbitals similarly distribute across the -8 eV to 4 eV energy range but with higher peak intensities than in the Valley-1Fe case. Crucially, the Fe(d) orbitals in the Top-1Fe configuration produce two prominent peaks at -0.62 eV and -0.73 eV, both situated in close proximity to the Fermi level. These energetic positions facilitate significant hybridization and electronic state contributions near the band edges. As a direct result, the presence of these Fe(d) peaks near the Fermi level closes the band gap entirely, transitioning the system from a narrow-gap semiconductor to a metallic state. The substantial density of Fe(d) states at the Fermi level enhances charge carrier density, electron mobility, and overall metallic behavior.

Additionally, the Top-1Fe configuration yields the highest adsorption energy of 10.73 eV, denoting it as the most thermodynamically favorable single-atom doping scenario within the ASnNR lattice. The pronounced interaction of Fe(d) states with host Sn orbitals not only alters the PDOS profile but also significantly enhances charge transfer activity in the vicinity

of the Fermi level, further facilitating gap closure. The disparity between the Valley-1Fe and top-1Fe configurations can be attributed to the spatial and electronic environment surrounding the dopant atom. In the valley position, the Fe atom occupies a relatively symmetric and electronically less constrained site, where hybridization with adjacent Sn atoms is spatially limited, resulting in Fe(d) states that remain localized and energetically distant from the Fermi level.

This limited interaction preserves a finite band gap. Conversely, the top position places the Fe atom in a more electronically active site with higher coordination to neighboring Sn atoms, increasing the probability of d–p hybridization and enabling the Fe(d) orbitals to strongly couple with conduction and valence states near the Fermi level. This coupling introduces mid-gap states, thereby narrowing and eventually closing the band gap. Further corroborating this explanation is the observation of bond length and bond angle variations in the optimized geometries. While both configurations maintain Sn–Fe bond lengths within the expected range ($\sim 2.55\ \overset{0}{A}$), the extent of structural distortion is more pronounced in top-1Fe, where enhanced Fe–Sn interactions lead to greater local rearrangements that favor electronic state redistribution.

These structural modifications contribute to the stabilization of the dopant and facilitate the overlap between Fe(d) and Sn(p) orbitals, a necessary condition for the observed metallic behavior. When extending the analysis to the scenario of 100%Fe substitution, where all Sn atoms within the ASnNR lattice are replaced by Fe atoms, the electronic and magnetic behaviors exhibit predictable trends. The system demonstrates a significantly reduced adsorption energy of -3.99 eV due to the absence of Sn atoms, while achieving the highest magnetic moment of 11.3 μB. The PDOS analysis reveals an increased contribution from Fe(s) orbitals and relatively minor deviations in Fe(d) and Fe(p) orbitals compared to single-atom doping cases. The system retains structural integrity through continuous Fe–Fe bonding, and the overlapping Fe(d) orbitals facilitate efficient electron exchange, enhancing metallic conductivity and electron mobility. These observations reaffirm the critical role of Fe(d) orbitals in determining the electronic structure and underline the importance of dopant positioning in tailoring the properties of ASnNRs for device applications.

In conclusion, this detailed computational study highlights the profound influence of dopant positioning on the electronic and magnetic properties of ASnNRs. The Valley-1Fe configuration preserves a narrow semiconducting band gap due to the localized and energetically distant positioning of Fe(d) states, whereas the top-1Fe configuration induces complete band gap closure as a result of prominent Fe(d) peaks near the Fermi level and stronger hybridization with Sn orbitals. These findings suggest that precise control over dopant positioning is essential for tuning the band structure and magnetic characteristics of stanene-based nanoribbons, offering strategic pathways for the development of customized electronic, optoelectronic, and spintronic devices. Future experimental and theoretical studies should explore the feasibility of selectively doping at specific lattice sites and assess the stability, synthesis, and device integration of these doped systems to fully exploit their potential in next-generation nanoscale applications.

If the ρ_{tot}, $\rho_{pristine}$, ρ_{Sn}, and ρ_{Fe} are the charge density of the Fe substituted ASnNR structures, pristine ASiNR, Sn atoms replaced by Fe adatoms in the pristine system, and isolated Fe adatoms, respectively and n is the number of the Fe substitution atoms as in Eq. 2:

$$\rho_{Form} = \rho_{tot} + \rho_{pristine} + n\rho_{Sn} - \rho_{Fe} \quad (2)$$

By combining the data from Table 2 and Fig. 6, we analyze the charge density distribution based on DFT calculations and their corresponding visualizations. The charge density is displayed on a blue-green-red (BGR) scale, ranging from -0.02 to 0.02 $e/(\overset{0}{A})^3$, with the selected charge density system corresponding to this range. The charge density maps, presented in both top and side views, show that the Fe atoms exhibit a predominantly negative charge density. This is attributed to the strong electron-withdrawing nature of Fe, which pulls charge from its surrounding environment, as indicated by the blue re-

Tab. 1: Calculation results of Fe doped with ASnNR substrate for different cases.

	Ortho	Para	Meta	Top-1Fe	Valley-1Fe	100 % Fe	Pristine
EForm	-6.13	-5.94	-8.25	-10.73	-6.13	-3.99	x
Buckl ($\overset{0}{A}$)	0.32	0.45	1	0.79	0.71	0.9	1
Sn-Sn ($\overset{0}{A}$)	2.83	2.73	2.82	2.81	2.82	x	2.82
Sn-Fe ($\overset{0}{A}$)	2.57	2.55	2.56	2.53	2.54	2.54	x
Fe-Fe ($\overset{0}{A}$)	2.11	x	x	x	x	x	x
Deg (°)	123.5	121.57	108.05	108.72	112.28	108.05	108.05
Mag (μB)	4	5.16	5.99	4.04	4	11.3	0
Eg (eV)	0.14	0.01	0.01	0.01	0.24	0.01	0.26

gions. In contrast, the Sn atoms, surrounded primarily by yellow regions, are either charge-neutral or contribute a small amount of charge to their neighboring atoms. This charge redistribution is consistent across the ortho, para, and meta doping configurations, as shown in Table 2, where the doped systems exhibit a reduced charge density compared to the pristine structure, with a charge density variation ρ_{Form} less than zero. Notably, the dark red regions around the Fe atoms in all three configurations suggest that Fe behaves as a charge donor rather than a charge acceptor. This observation is further supported by the cross-sectional charge density profiles of the Fe atoms, reinforcing their role in charge transfer within the doped system.

In the overlapping region of the charge clouds, the hybridization between the Fe(d) and Sn(p) orbitals facilitates a charge exchange, creating "trap states" that pull the Fermi level toward the valence or conduction band, ultimately narrowing the band gap. This phenomenon is particularly evident in the Fe-doped configurations, where the interaction between the d-orbitals of Fe and p-orbitals of Sn leads to the formation of localized states that influence the electronic structure. Typically, the electron density remains at a neutral level in the pristine structure, with no significant charge donation or acceptance observed when considering cross-sections consisting only of Sn-Sn bonds without any Fe atoms.

However, following doping, the change in charge density ($\Delta\rho > 0$) does not necessarily correspond to an increase in the band gap width, as observed in the Top-1Fe, Valley-1Fe, and 100% Fe doping configurations. Instead, the electronic structure undergoes a rearrangement primarily driven by the contributions from Fe(d) and Fe(s) orbitals, which influence the charge distribution within the material. The hybridization and subsequent charge transfer between Fe and Sn orbitals not only alter the local electronic states but also contribute to the renormalization of the band gap, lowering its energy.

This charge redistribution and hybridization effect are crucial in stabilizing the new crystal structure after doping. The presence of Sn(p) and Fe(d) orbitals plays an essential role in this stabilization process by facilitating the exchange of charge between the two atom types, which results in a significant modification of the material's electronic properties. As a consequence, rather than expanding, the band gap is reduced due to the enhanced overlap of the Fe(d) and Sn(p) orbitals, which enhances electron mobility and makes the material more conducive to electron transport. This interplay of orbital interactions and charge transfer serves as a key factor in the structural and electronic stability of the Fe-doped systems, suggesting their potential for applications in semiconductor and spintronic devices.

3.3. Experimental Directions

The DC magnetron sputtering method is one of the widely used deposition techniques for thin film fabrication, particularly for metals, oxides, and magnetic compounds, through the

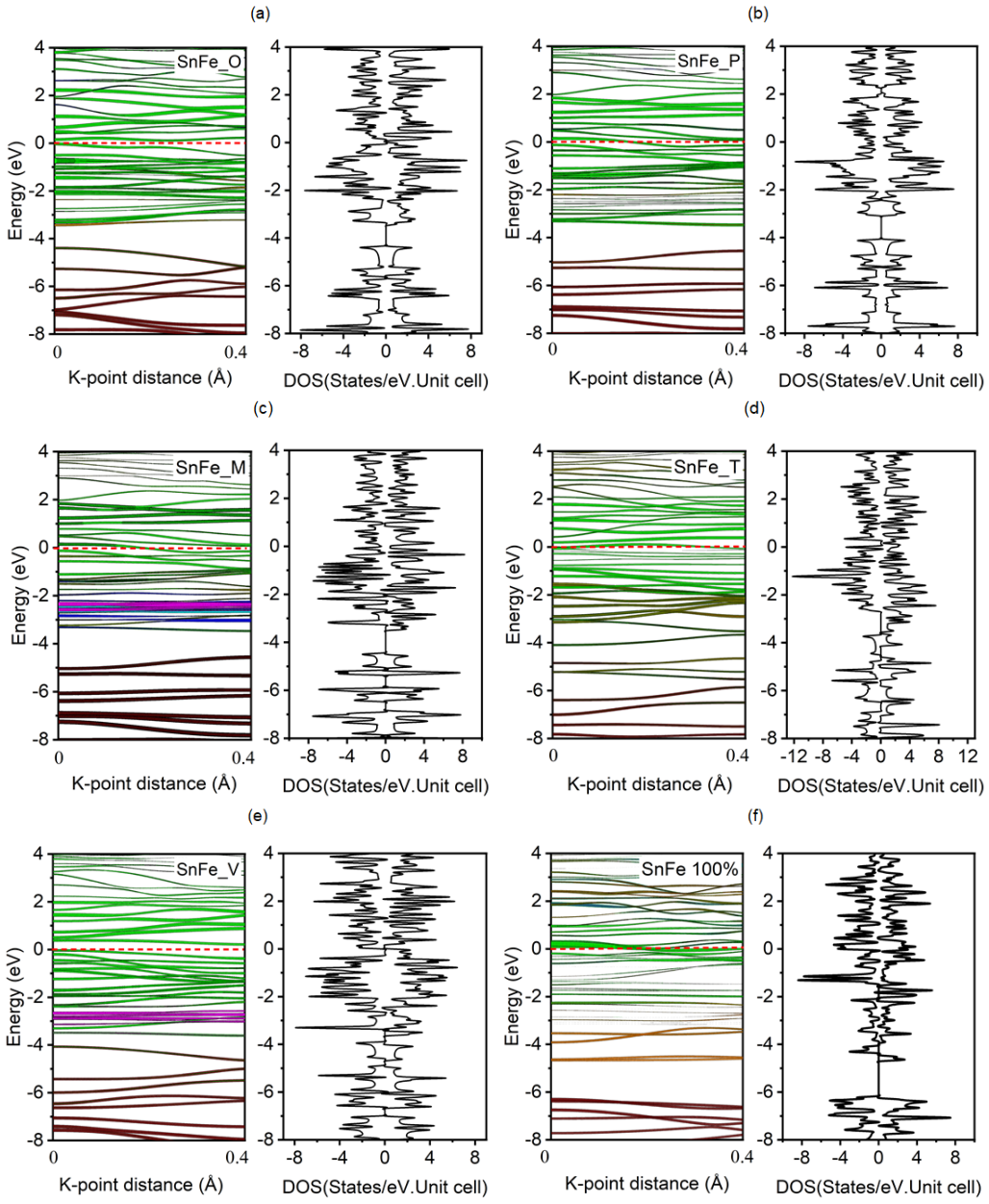

Fig. 5: The structure BAND and DOS states of (a) Ortho, (b) Para, (c) Meta, (d) Top-1Fe, (e) Valley-1Fe, and SnFe 100%.

use of plasma to sputter atoms or molecules from a target onto a substrate. This method can be utilized to dope Fe into Sn in studies and applications related to Stanene or other thin films. Application of DC Magnetron Sputtering in Fe Doping into Sn: DC magnetron sputtering can be applied to dope Fe into Sn through the following steps: i) Fabrication of Sn Thin Film: Initially, a thin Sn film needs to be prepared on the substrate. DC magnetron sputtering can be used to deposit a thin Sn layer by sputtering from an Sn target (typically a metal Sn target) in an inert gas environment like argon. This creates a Sn film on the substrate with the

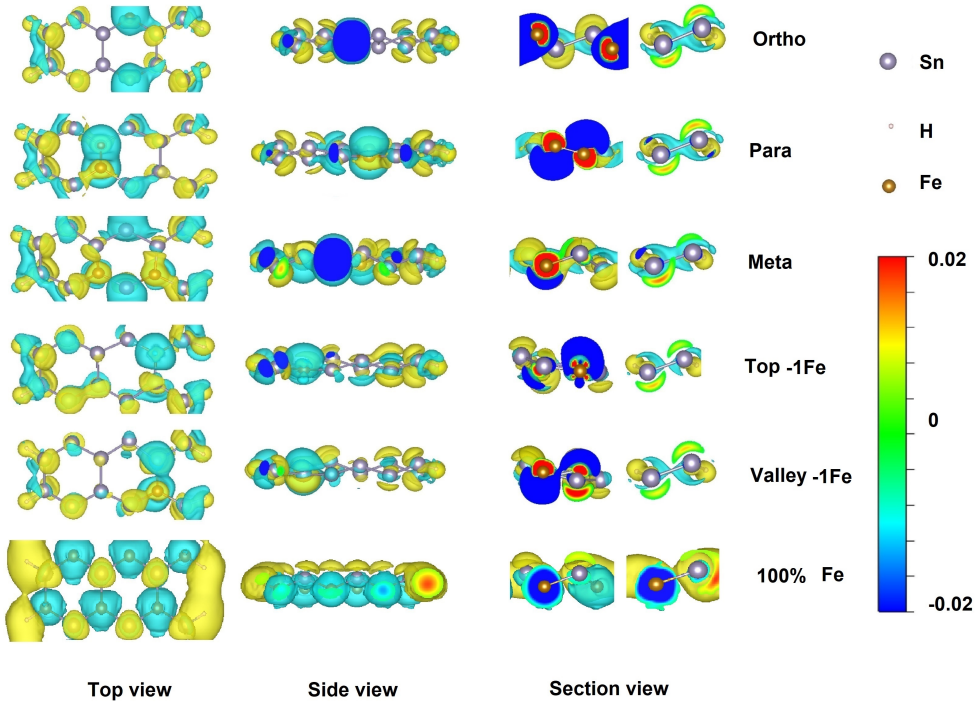

Fig. 6: Initial structure of Fe doped cases with ASnNRs.

required thickness and quality, ii) Fe Doping into Sn: After the Sn thin film is deposited, the next step is doping Fe into the Sn layer. In this case, DC magnetron sputtering can be employed using an Fe target. This process will sputter Fe atoms onto the Sn film, causing Fe to integrate into the Sn structure through vapor phase deposition, iii) Control of Fe Doping Ratio: The ratio of Fe doping into Sn can be controlled by adjusting the sputtering conditions such as sputtering current density, pressure inside the vacuum chamber, and sputtering time. It is also possible to adjust the ratio of argon and oxygen gases (if necessary) to precisely control the doping process, iv) Formation of Fe/Sn Doped Structure: Once the sputtering process is complete, the Fe/Sn material will have a doping structure, where Fe atoms are incorporated into the Sn matrix, creating Fe doping at specific sites, which may be either uniform or non-uniform depending on the doping conditions.

4. Conclusion

In this study, we investigated the effects of Fe atom substitution on the electronic and magnetic properties of armchair stanene nanoribbons. Six different doping configurations, including top, valley, ortho, meta, and para positions, were considered by replacing Sn atoms with Fe. The results reveal that Fe doping induces significant modifications in the band structure, primarily through charge transfer and bond formation with neighboring atoms. The most notable outcome is the reduction of the band gap compared to the pristine ASnNR, which possesses a calculated band gap of 0.26 eV, characteristic of a narrow-gap semiconductor. Fe doping enhances the charge density around the Fermi level, resulting in a substantial narrowing of the band gap in most configurations. In particular, top, ortho, and para substitutions reduce the band gap to nearly 0 eV, indicating a transition to metallic or semimetallic behavior. In contrast, the

Tab. 2: Convergence study of numerical results with respective number of elements used for a spherical thin shell.

Positions	Charge density	Orbitals s $(e/(\overset{0}{A})^3)$	Orbitals p$(e/(\overset{0}{A})^3)$	Orbitals d$(e/(\overset{0}{A})^3)$
Ortho	ρ_P	15.51	15.25	0.63
	ρ_X	0.82	0.16	12.54
	ρ_X+P	14.22	13.03	13.02
	$\Delta\rho$	-1.06	-1.19	-0.07
	ρ_P	15.51	15.25	0.63
Para	ρ_X	0.82	0.16	12.52
	ρ_X+P	14.21	13.19	12.87
	$\Delta\rho$	-1.06	-1.11	-0.14
Meta	ρ_P	15.51	15.25	0.63
	ρ_X	0.82	0.16	12.52
	ρ_X+P	14.15	12.45	12.88
	$\Delta\rho$	-1.09	-1.48	-0.13
Top-1Fe	ρ_P	14.38	13.35	0.54
	ρ_X	0.45	0	5.96
	ρ_X+P	15.06	14.51	6.78
	$\Delta\rho$	0.23	1.16	0.28
Valley-1Fe	ρ_P	14.55	12.96	0.65
	ρ_X	0.45	0	5.96
	ρ_X+P	15.07	14.44	6.78
	$\Delta\rho$	0.07	1.48	0.17
100% Fe	ρ_P	8.47	5.1	0.06
	ρ_X	-0.47	-0.08	19.28
	ρ_X+P	10.89	6.17	26.04
	$\Delta\rho$	0.48	0.19	1.12

valley-1Fe configuration maintains a narrow band gap of 0.24 eV due to limited electron exchange at this lower atomic position, where interaction with surrounding atoms is less significant. In addition to electronic alterations, Fe doping induces strong magnetism in all configurations, attributed to the magnetic moments of Fe atoms arising from their partially filled 3d orbitals. Notably, the configuration with 100% Fe substitution achieves the highest total magnetic moment of 11.3 µB, suggesting ferromagnetic behavior. This is of particular interest for spintronic applications, where control over electron spin is critical. In conclusion, the 100% Fe substituted ASnNR, exhibiting a zero band gap (Eg = 0 eV), behaves metallically, rendering it unsuitable for active semiconductor components such as transistors or diodes but highly promising for electronic applications requiring efficient charge transport. It can serve as a conductive electrode, interconnect in nanoelectronic circuits, or as an interfacial buffer layer in heterostructure devices. Furthermore, if the Fe dopants retain magnetic ordering, the material holds potential for spintronic devices such as spin valves and tunneling magnetoresistance systems. Its metallic conductivity and surface sensitivity also make it a good candidate for gas sensing applications. Nevertheless, structural stability and chemical durability must be further examined to ensure practical applicability.

5. Acknowledgement

With this project, we would like to thank you used resources of the high-performance com-

puter cluster (HPCC) at Thu Dau Mot University, Binh Duong Province, Vietnam.

References

[1] J. Abraham, R. Arunima, K.C. Nimitha, S.C. George, and S. Thomas. One-dimensional (1d) nanomaterials: Nanorods and nanowires; nanoscale processing. *Nanoscale Process. Micro Nano Technol.*, pages 71–101, 2021.

[2] X. Li, J. Huang, Y. Zhang, and L. Shi. 1d nanoribbons of 2d materials. *Prog. Chem.*, 35(1):88–104, 2023.

[3] M.R.Sahudin, M.d Zourob, M.H.N. Akashah, R.A. Rani, and S.R. Makhsin. Physical properties of graphene. *J. Mech. Eng.*, 12(1):225–267, 2023.

[4] C. Zhao, R. Wang, B. Fang, H. Liang, R. Li, S. Li, Ya Xiong, Y. Shao, B. Ni, R. Wang, B. Xu, S. Feng, and R. Mo. Macroscopic assembly of 2d materials for energy storage and seawater desalination. *Iscience*, 26(12):1084367, 2014.

[5] J.K. Lyu, S.F. Zhang, C.W Zhang, and P.J. Wang. Stanene: A promising material for new electronic and spintronic applications. *Condens. Matter Physics, Ann. der Physik*, 531(10):1900017, 2019.

[6] M. Ezawa. Monolayer topological insulators: Silicene, germanene, and stanene. *The Phys. Soc. Jpn.*, 84:121003, 2015.

[7] B.Peng, H. Zhang, H. Shao, Y. Xu, X. Zhang, and H. Zhu. Low lattice thermal conductivity of stanene. *Sci. Reports*, 6):20225, 2018.

[8] Y. Yang, H. Zhang, L. Song, and Z. Liu. Adsorption of gas molecules on the defective stanene nanosheets with single vacancy: A DFT study. *Appl. Surf. Sci.*, 512(1):145727, 2020.

[9] K. Sheng, H.K. Yuan, H. Chen, and Z.Y. Wang. Adsorption of single alkali-metal atoms (Li, Na, K) over the edge-passivated zigzag blue phosphorene nanoribbons. *J. Phys. Chem. Solids*, 146:109623, 2020.

[10] A. Ling-yan, C. Chun-Rui, Y. Liu, and H. Liu. Tuning the electronic properties and band gap engineering in stanene monolayers via codoping of mn and Al/P/Ga/As atoms: A DFT study. *Comput. Theor. Chem.*, 1188:112939, 2020.

[11] X. Dan-Xu, R. Ceng-Ceng, Z. Shu-Feng, F. Yong, C. Xin-Lian, Z. Chang-Wen, and W. Pei-Ji. Tunable electronic and magnetic properties in stanene by 3d transition metal atoms absorption. *Superlattices Microstruct.*, 103:139–144, 2017.

[12] P. Garg, I.Choudhuria, and B. Pathak. Stanene based gas sensors: Effect of spin-orbit coupling. *Phys. Chem. Chem. Phys*, 19:31325–31334, 2017.

[13] T.T. Nguyen, C.P. Tran, and V.N. Hoang. Electromagnetic and optical properties of na, mg, and al-adsorbed stanene nanoribbons: potential applications. *J. Physics: Condens. Matter*, 37(11):115901, 2025.

[14] T.T. Nguyen, C.P. Tran, and V.N. Hoang. Adsorption of co, f2, and no2 on stanene nanoribbons: Optoelectronic, properties and sensing applications. *Chem. Phys.*, 594:112668, 2025.

[15] Q. Zhou, L. Wang, W.Ju, Y. Yong, S. Wu, S. Cai, and P. Li. Quantum capacitance of vacancy-defected and co-doped stanene for supercapacitor electrodes: A theoretical study. *Electrochimica Acta*, 433:141261, 2022.

[16] N. Kumar, L. Ye-Shun, I. Jang, L. Yen-Hui, C. Chia-Ju, L. Tzu-Hsuan, J. Horng-Tay, C. Po-Yao, and H. Pin-Jui. Atomic-scale magnetic doping of monolayer stanene by revealing kondo effect from self-assembled fe spin entities. *npj Quantum Mater.*, 9:37, 2024.

[17] D. Xian-Qi andZ. Ming-Yu Zhao, Z.Ru-Meng, and L. Wei. Biaxial tensile strain modulates magnetic properties of the 3d transition metal doped stanen. *Superlattices Microstruct.*, 106:33–49, 2017.

[18] J. Hafner. Materials simulations using vasp—a quantum perspective to materials science. *Comput. Phys. Commun.*, 177(1-2):6–13, 2007.

[19] J.C. Sancho-Garcıa, J.L. Brédas, and J. Cornil. Assessment of the reliability of the perdew–burke–ernzerhof functionals in the determination of torsional potentials in π-conjugated molecules. *Chem. Phys. Lett.*, 377(1-2):63–68, 2003.

[20] C. Filippi and X. Gonze. Generalized gradient approximations to density functional theory: Comparison with exact results. *Theor. Comput. Chem.*, 4:1–32, 1996.

[21] T. Rangel, D. Caliste, L. Genovese, and M. Torrent. A wavelet-based projector augmented-wave (paw) method: Reaching frozen-core all-electron precision with a systematic, adaptive and localized wavelet basis set. *Comput. Phys. Commun.*, 208:1–8, 2016.

[22] Y. Wang, P. Wisesa, A. Balasubramanian, S. Dwaraknath, and T. Mueller. Rapid generation of optimal generalized monkhorst-pack grids. *Comput. Mater. Sci.*, 187:110100, 2021.

[23] T. Ishida and K. Ohno. Force analysis by molecular orbitals — partition of the hellmann–feynman force into one-electron orbital contributions. *J. Mol. Struct. THEOCHEM*, 461–462:335–349, 1999.

[24] Z.P. Madzarevic, S. Shahid, K. Nijmeijer, and T.J. Dingemans. The role of ortho-, meta- and para-substitutions in the main-chain structure of poly(etherimide)s and the effects on co2/ch4 gas separation performance. *Sep. Purif. Technol.*, 210:242–250, 2019.

[25] T.T. Nguyen, V.N. Hoang, T.P.T. Huynh, D.K. Nguyen, and V.O. Vo. Diverse structural and electronic properties of carbon-substituted armchair silicene nanoribbons: A first-principles study. *Phys. E: Low dimensional Syst. Nanostructures*, 142:115309, 2022.

[26] C. Kraka and C. Dieter. Ortho-, meta-, and para-benzyne. a comparative ccsd (t) investigation. *Chem. Phys. Lett.*, 216(3–6):333–340, 1993.

About Authors

Nguyen Thanh TUNG is a lecturer at Institute of Engineering Technology, Thu Dau Mot University, Binh Duong Province, Vietnam. He is studying for a PhD in Computational Science at Ton Duc Thang University, Vietnam. Graduated from pedagogical university in physics in 1991 at Can Tho University. Graduated with a master's degree in Optics from the University of Natural Sciences, Ho Chi Minh City National University, Vietnam in 2003. Has many studies in the field of simulated and experimental materials science.

Tran Cong PHONG obtained a PhD in Theoretical Physics and Mathematical Physics from the National University of Hanoi in 1999 and attained the rank of professor in 2012. Engaged in research at the Institute for Advanced Study in Technology, Ton Duc Thang University. The primary study domains encompass materials derived from low-dimensional structures, nanostructures, especially semiconductors, and functional materials and structures.